22nd International Conference on Sustainable Energy Technologies
Kuala Lumpur, Malaysia, 13 to 15 August 2026 · ISBN 978-1-995850-00-9 · ISSN 2978-4387

CONFERENCE PAPER · AI & RENEWABLE SYSTEMS

Machine-Learning-Assisted Design and Analysis of an Integrated Allam Cycle-CO_2 Energy Storage System

Yingzong Liang[1*], Jialuan Zhang[2], Xianglong Luo[1]

[1] School of Materials and Energy, Guangdong University of Technology, Guangzhou, China
[2] Guangdong R & D Center for Technological Economy, Guangzhou, China

RECEIVED 12 June 2026 · REVISED 2 July 2026 · ACCEPTED 13 July 2026
PRESENTED 13 to 15 August 2026 · PUBLISHED 23 November 2026

ABSTRACT

This paper proposes an integrated system that couples an Allam cycle with CO_2 energy storage. The system can flexibly adjust the CO_2 stream routing according to the availability of environmental cooling, thereby reducing the power consumption of the compression process. During the charging stage, CO_2 is pressurised by the pump in the Allam cycle and stored in a high-pressure tank. During the discharging stage, the storage system further improves thermal efficiency and round-trip efficiency by integrating waste-heat recovery from the Allam cycle with the utilisation of environmental cooling. Because the integrated Allam cycle-CO_2 energy storage system has a complex configuration and requires time-consuming numerical calculations, a machine-learning method is introduced to rapidly predict key performance indicators, including thermal efficiency, round-trip efficiency, and net specific work under varying key parameters, thus substantially improving the efficiency of performance evaluation. The results show that, under a low-pressure tank pressure of 7.4 MPa, a high-pressure tank pressure of 30.3 MPa, and a tank temperature of 20 °C, the thermal efficiency of the integrated system is 3.57 percentage points higher than that of the conventional Allam cycle, the round-trip efficiency of the CO_2 energy storage system reaches 85.74%, and the net specific work increases by 6.28%.

KEYWORDS Allam cycle, CO_2 energy storage, System integration, Machine learning

1. Introduction

In recent years, the large-scale consumption of fossil fuels has led to substantial greenhouse gas emissions, becoming an important driver of global climate change (Crippa *et al.* 2022). Against the background of the low-carbon energy transition, developing advanced energy systems with both high efficiency and low carbon emissions has become a major research focus. The Allam cycle is a novel power cycle using supercritical CO_2 as the primary working fluid. It can achieve efficient CO_2 capture during hydrocarbon-fueled power generation and therefore shows strong application prospects in clean fossil-fuel utilization and carbon emission reduction. Allam *et al.* (2013) first proposed the cycle concept in 2013. Scaccabarozzi *et al.* (2016) subsequently conducted systematic thermodynamic analysis and optimization, showing that the maximum cycle efficiency could reach 54.80%. Meanwhile, as the demand for peak shaving and frequency regulation in power systems continues to grow, energy storage technologies are playing an increasingly important role in improving system flexibility and overall energy-utilization efficiency. Carbon dioxide energy storage systems (CCES) have attracted broad attention owing to their relatively high energy storage density and engineering application potential. Sun *et al.* (2021) proposed a low-pressure liquid CO_2 energy storage system, achieving a round-trip efficiency and energy storage density of 51.45% and

* Corresponding author. Email address: yliang@gdut.edu.cn (Yingzong Liang)

© 2026 The Author(s).
Published by Caravel Press.

doi.org/10.65582/set.2026.032

22.21 kWh/m³, respectively. Li *et al.* (2025) further proposed a high-temperature liquid CO_2 energy storage system, achieving a round-trip efficiency of 66.68% and an energy storage density of 28.57 kWh/m³ under specified operating conditions. Although positive progress has been made, existing studies still mainly focus on stand-alone CO_2 energy storage systems, while their integration with efficient CO_2 power cycles remains insufficiently investigated.

Accordingly, this paper proposes an integrated Allam cycle-CO_2 energy storage system. Through case analysis and sensitivity analysis, the feasibility of the proposed scheme is systematically evaluated, and the effects of key operating parameters on system performance are revealed. In addition, to address the high computational cost of solving the integrated system under multi-parameter operating conditions, a machine-learning surrogate model is developed to rapidly predict key performance indicators and provide an efficient computational tool for subsequent system optimization.

2. System Description

The proposed integrated Allam cycle-CO_2 energy storage system consists of a CO_2 energy storage subsystem and an Allam cycle subsystem, and operates in three modes: normal, charging, and discharging.

The integrated system mainly consists of a natural gas compressor (Comp-NG), an oxygen compressor (Comp-O_2), three-stage CO_2 compressors (Comp1-Comp3), a turbine (Tur), a combustor (Comb), a pump (Pump), a condenser, an air separation unit (ASU), a gas-liquid separator (Sep), a low-pressure tank (LPT), a high-pressure tank (HPT), a recuperator (Regen), a CO_2 processing unit (CPU), and valves. The CO_2 flow direction can be adjusted according to the availability of ambient cooling. When cooling capacity is insufficient, the system maintains power generation; during low-load periods, it switches to the charging mode and stores more CO_2 in the high-pressure tank; when electricity demand increases, it switches to the discharging mode and releases CO_2 from the high-pressure tank to increase power output. This enables grid peak shaving and enhances the system adaptability to long-term ambient-temperature fluctuations.

As shown in Figure 1, in the normal mode, the system operates according to the Allam cycle. The fuel is compressed (1→2) and then enters the combustor, where it is mixed and combusted with the preheated oxidant stream (OX-2). Meanwhile, a recycled CO_2 stream (CC-2) is introduced to regulate the combustion temperature. The high-temperature flue gas produced by combustion enters the turbine for expansion and power generation (3→4). Because the flue-gas temperature is high, a recycled CO_2 cooling stream (CT-2) is used to cool the turbine. The turbine exhaust then enters the recuperator to preheat the recycled CO_2 streams (CC-1 and CT-1) and the oxidant stream (OX-1) (4→5), after which it enters the gas-liquid separator to obtain high-purity CO_2 (5→6). The excess CO_2 is captured by the CPU and discharged from the system, while the remaining recycled CO_2 enters the first-stage compressor (Comp1) and is compressed to 7.4 MPa (7→8). The compressed CO_2 follows different routes depending on the availability of ambient cooling. When ambient cooling is insufficient, the CO_2 undergoes an intercooled compression process (8→13), after which part of the recycled CO_2 mixes with the oxygen stream (O-1) from the ASU and then enters the subsequent process after pressurization by the oxygen compressor. When ambient cooling is sufficient, the CO_2 is first condensed into liquid in the condenser (14→15), then further pressurized in the intercooled pump section (15→16), and mixed with the oxygen stream (O-2). The valves are used to control the on/off state and route switching of the CO_2 streams.

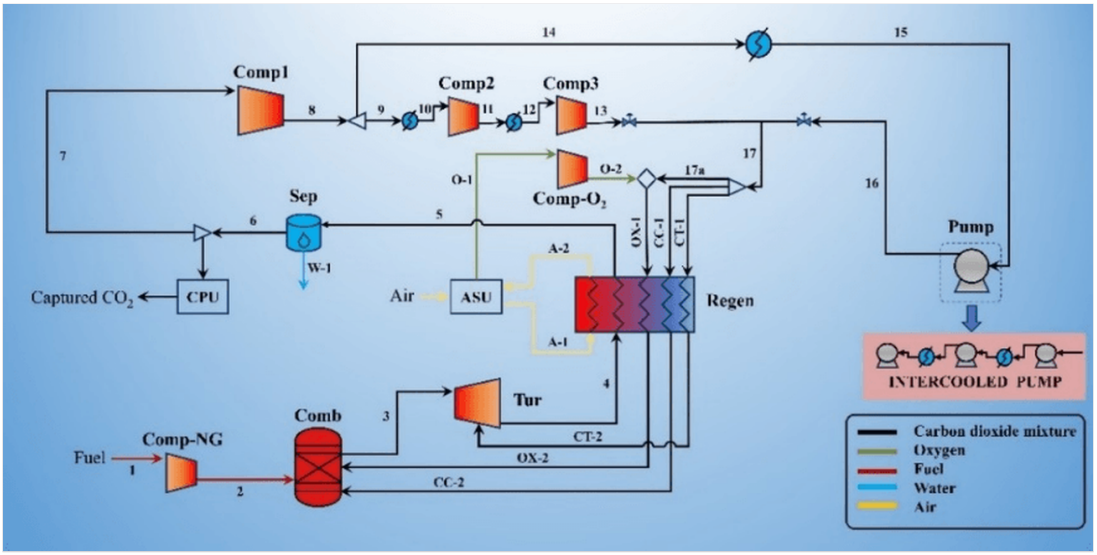

Figure 1. Normal mode.

The charging mode is shown in Figure 2. CO_2 in the low-pressure tank (LPT) is pressurized by the pump to a high pressure (S-2→17) and then stored in the high-pressure tank (HPT) (S-3). Compared with the normal mode, the CO_2 flow rate through the pump increases in the charging mode, while the other processes in the Allam cycle subsystem remain unchanged.

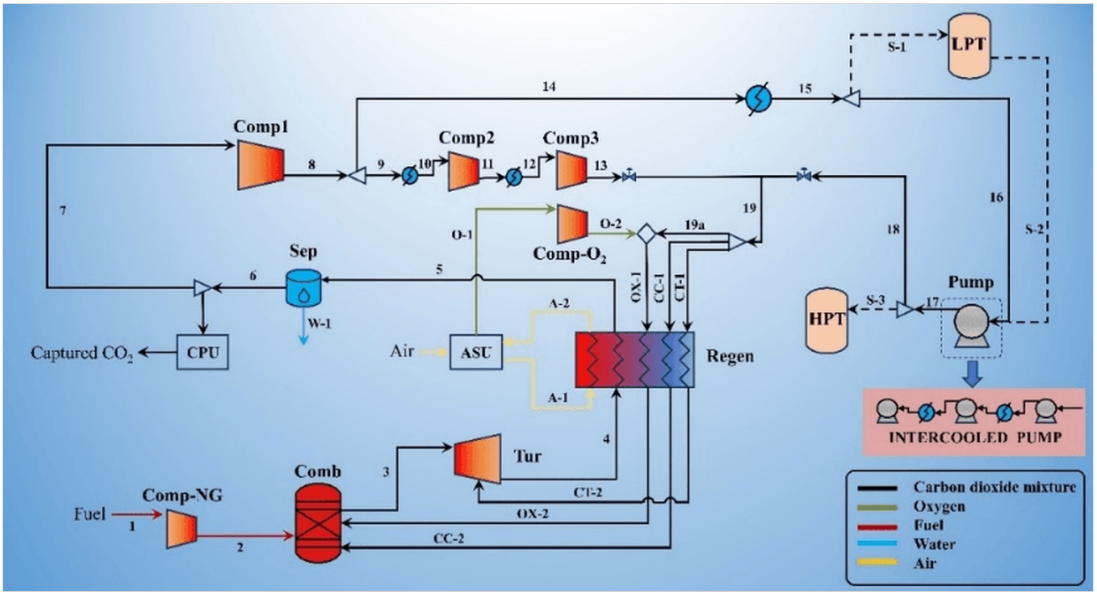

Figure 2. Charging mode.

The discharging mode is shown in Figure 3. CO_2 in the high-pressure tank (HPT) is released, mixed with the CO_2 at the pump outlet, and then introduced into the Allam cycle. Compared with the normal mode, the CO_2 flow rates of the streams in the Allam cycle, except for the stream passing through the pump, increase in the discharging mode, enabling the turbine to produce additional power output. At the same time, because the pump power consumption remains nearly unchanged, the net power output of the system increases. The additional CO_2 introduced during discharging is eventually condensed and returned to the low-pressure tank (LPT), completing the circulation of the energy storage medium.

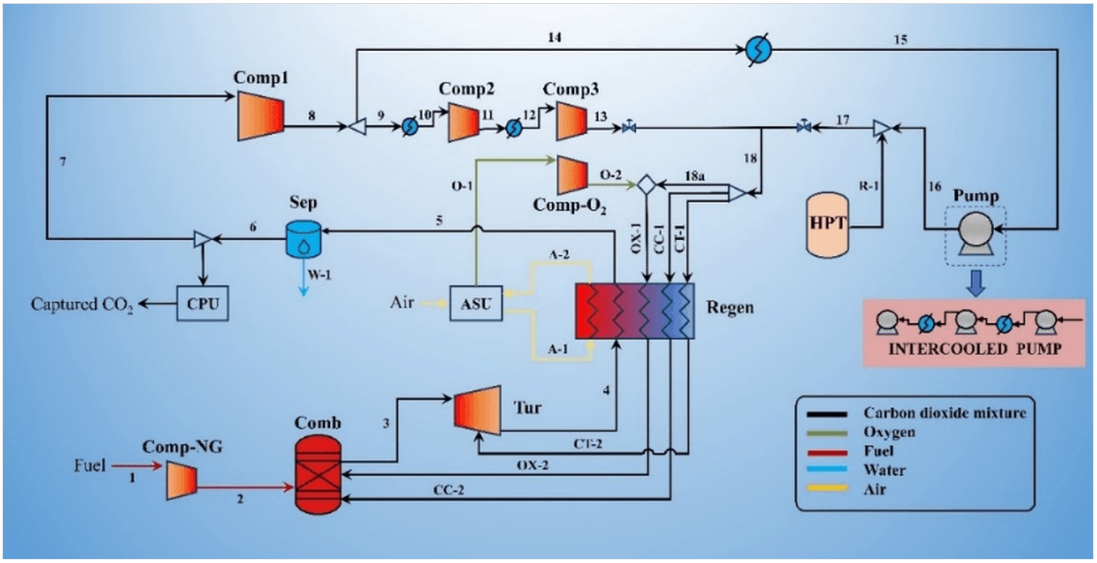

Figure 3. Discharging mode.

3. Mathematical Model

3.1. Basic Assumptions

This section establishes the thermodynamic mathematical model of the system. Model construction and calculation are implemented in Python, and the thermophysical properties of the working fluids are obtained by calling CoolProp. Each component in the model satisfies the mass and energy conservation equations. The main assumptions are as follows:

1. The system operates under steady-state conditions;
2. Heat loss, pressure drop, and mass leakage in all connecting pipelines are neglected;
3. The operating modes can switch instantaneously, and the influence of the switching process on system performance is neglected;
4. Changes in the kinetic and potential energies of the working fluid in each component are neglected;
5. Heat loss between heat exchangers and the environment is neglected;
6. The mass flow rates during the charging and discharging processes are equal.

3.2. Mass and Energy Conservation

For an arbitrary control volume under steady-state conditions, the mass conservation equation is

$$\sum \dot{m}_{\text{in}} = \sum \dot{m}_{\text{out}} \tag{1}$$

where $\dot{m}$ is the mass flow rate, kg/s.

The energy conservation equation for the control volume is

$$\sum \dot{m}_{\text{in}} h_{\text{in}} + \dot{Q} - \dot{W} = \sum \dot{m}_{\text{out}} h_{\text{out}} \tag{2}$$

where h is specific enthalpy, kJ/kg; $\dot{Q}$ is the heat transfer between the control volume and its surroundings, kW; and $\dot{W}$ is the power output from the control volume, kW.

3.3. Recuperator

The recuperator is modeled as a multi-stream heat exchanger. Each stream in the recuperator satisfies the mass conservation relation

$$\dot{m}_{j,\mathrm{in}} = \dot{m}_{j,\mathrm{out}} \qquad j = 1,\ 2,\ \ldots,\ n \tag{3}$$

where n is the number of fluid branches in the recuperator.

When heat loss between the recuperator and the environment is neglected, the overall energy conservation relation of the recuperator is

$$\sum_{h} \dot{m}_h \left(h_{h,\mathrm{in}} - h_{h,\mathrm{out}}\right) = \sum_{c} \dot{m}_c \left(h_{c,\mathrm{out}} - h_{c,\mathrm{in}}\right) \tag{4}$$

where subscript h denotes the hot fluid and subscript c denotes the cold fluid.

Considering the significant variation in working-fluid properties with temperature and pressure inside the recuperator, this paper follows the treatment of Scaccabarozzi *et al.* (2016) and discretizes the recuperator along the flow direction into N elemental segments to improve the accuracy of heat-transfer calculations. For the kth elemental segment,

$$\sum_{h} \dot{m}_h \left(h_{h,k} - h_{h,k+1}\right) = \sum_{c} \dot{m}_c \left(h_{c,k+1} - h_{c,k}\right) \qquad k = 1,\ 2,\ \ldots,\ N \tag{5}$$

For the recuperator, it is assumed that all hot streams at the same cross-section have the same temperature and that all cold streams at the same cross-section also have the same temperature. The minimum temperature difference in the main body of the recuperator is set to 5 K. Because the heat-transfer capability at the hot end is relatively weak, the minimum hot-end temperature difference is set to 20 K. For the kth discrete node, the temperature difference can be defined as

$$T_{h,k} - T_{c,k} \geq \Delta T_{\min} \qquad k = 1,\ 2,\ \ldots,\ N+1 \tag{6}$$

The above temperature-difference constraints ensure that the minimum temperature difference between the hot and cold streams is not lower than the specified value.

3.4. Air Separation Unit

The air separation unit is not modeled in detail in this paper; instead, the ASU is treated as a black-box model. The specific energy consumption of the ASU is assumed to be 1391 kJ/kg O_2, and it supplies oxygen at 15 °C and 120 bar to the combustor as the oxidant.

3.5. Combustor

The combustor model is established based on mass and energy conservation. The combustor is treated as an adiabatic component without heat exchange with the surroundings. Complete combustion of the fuel in the combustor is also assumed, and the thermal energy of the fuel is provided by its chemical reaction heat. When the lower heating value of the fuel is used,

$$\dot{Q}_{\mathrm{fuel}} = \dot{m}_{\mathrm{fuel}}\,\mathrm{LHV} \tag{7}$$

where subscript fuel denotes the fuel.

3.6. Turbine Cooling Model

A turbine cooling model is used to describe the expansion process of high-temperature flue gas in the turbine. The turbine inlet working fluid is the flue gas from the combustor outlet, and the cooling medium is the recycled CO_2 cooling stream. The total number of stages in the model is N. The first $N-1$ stages use a uniform pressure ratio, and the final stage expands to the specified outlet pressure. Iterative solution is performed so that the inlet temperature of the final stage reaches the maximum allowable turbine blade temperature of 860 °C.

3.7. Thermodynamic Analysis

This paper proposes a method for calculating the round-trip efficiency (RTE) of the integrated Allam cycle-CO_2 energy storage system. In the charging mode, the increase in CO_2 flow rate leads to higher compression power consumption; the additional compression work is defined as the charging work input, namely the difference between the compression work in the charging mode and that in the normal mode. In the discharging mode, CO_2 in the high-pressure tank is released and introduced into the Allam cycle. Because this portion of CO_2 participates in waste-heat recovery and expansion work within the cycle, the system obtains additional power output. To distinguish the contribution caused by the increase in fuel heat input, the difference between the total heat input in the discharging mode and that in the normal Allam cycle is defined as the additional fuel heat input. After subtracting the contribution corresponding to this additional fuel heat input from the additional net power output during discharging, the effective net work benefit generated by releasing CO_2 from the high-pressure tank is obtained, and the system RTE is then calculated. The subscripts “n”, “char”, and “dis” denote parameters in the normal, charging, and discharging modes, respectively.

$$\Delta \dot{Q}_{\mathrm{dis}} = \dot{Q}_{\mathrm{dis}} - \dot{Q}_{\mathrm{n}} \tag{8}$$

$$\Delta \dot{W}_{\mathrm{dis}} = \Delta \dot{Q}_{\mathrm{dis}} \cdot \eta_{\mathrm{n}} \tag{9}$$

$$\Delta \dot{E}_{\mathrm{char}} = \dot{W}_{\mathrm{c,char}} - \dot{W}_{\mathrm{c,n}} \tag{10}$$

$$\Delta \dot{E}_{\mathrm{dis}} = \dot{W}_{\mathrm{r,dis}} - \Delta \dot{W}_{\mathrm{dis}} \tag{11}$$

$$\mathrm{RTE} = \frac{\Delta \dot{E}_{\mathrm{dis}}}{\Delta \dot{E}_{\mathrm{char}}} \tag{12}$$

The net electrical efficiency represents the net electric power output obtained per unit chemical energy input of the fuel and is defined as

$$\eta_{\mathrm{ele}} = \frac{\dot{W}_{\mathrm{net,ele}}}{\dot{Q}_{\mathrm{fuel}}} \tag{13}$$

where $\dot{W}_{\mathrm{net,\,ele}}$ is the net electric power output of the system, MW.

The net electric power output is usually expressed as the turbine generator output minus the power consumption of all system equipment, and can be written as

$$\dot{W}_{\mathrm{net,ele}} = \phi\left(\dot{W}_{\mathrm{Tur}} - \dot{W}_{\mathrm{Comp}} - \dot{W}_{\mathrm{Pump}} - \dot{W}_{\mathrm{ASU}}\right) \tag{14}$$

where ϕ is the generator efficiency; $\dot{W}_{\mathrm{Tur}}$ is the turbine output power, kW; $\dot{W}_{\mathrm{Comp}}$ is the compressor power consumption in the system, kW; $\dot{W}_{\mathrm{Pump}}$ is the pump power consumption in the system, kW; and $\dot{W}_{\mathrm{ASU}}$ is the ASU power consumption, kW.

The net specific work represents the net electric power output per unit turbine inlet mass flow rate and is defined as

$$\omega = \frac{\dot{W}_{\mathrm{net,ele}}}{\dot{m}_{\mathrm{Tur}}} \tag{15}$$

where ω is the net specific work, kJ/kg; and $\dot{m}_{\mathrm{Tur}}$ is the turbine inlet mass flow rate, kg/s.

4. Machine Learning

Because calculating the RTE of the integrated Allam cycle-CO_2 energy storage system involves complex property calls and iterative solution procedures, the computation time for a single operating condition is relatively long and cannot readily meet the requirements of large-scale parametric analysis and optimization design. Therefore, a machine-learning surrogate model is constructed based on the high-fidelity thermodynamic model. A supervised learning dataset is generated through parameter sampling and point-by-point calculation, and XGBoost (Extreme Gradient Boosting) is selected to rapidly predict key performance indicators, including the round-trip efficiency, net electrical efficiency, and net specific work. Five parameters are selected as input features of the model: turbine cooling-flow temperature, tank mass flow rate, turbine outlet pressure, first-stage compressor inlet temperature, and first-stage compressor outlet pressure. These parameters can effectively represent the system operating state and have important effects on the round-trip efficiency, net electrical efficiency, and net specific work. To verify the predictive capability of the model, 100 independent operating-condition datasets are used for testing, and the results are visualized using scatter plots of predicted values against reference values, as shown in Figure 4.

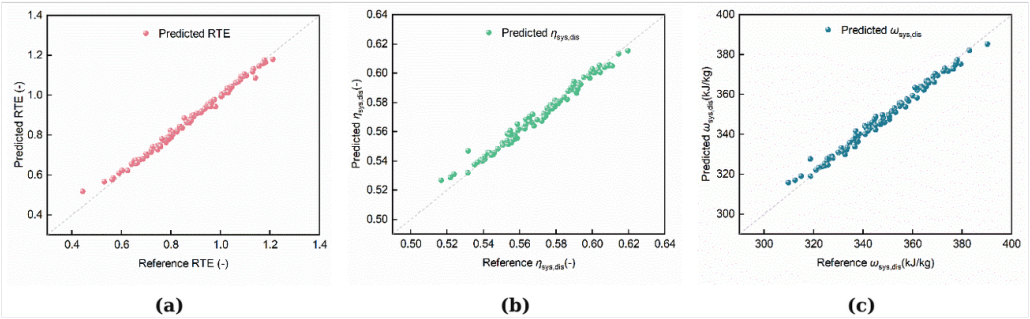

Figure 4. Validation results of output variables of the surrogate model: (a) round-trip efficiency; (b) net electrical efficiency; (c) net specific work.

To quantify the improvement in computational efficiency provided by the machine-learning surrogate model, this paper evaluates the computational cost of generating the dataset using the high-fidelity thermodynamic model. A total of 500 sample datasets are generated, requiring a cumulative calculation time of approximately 20.8 h; thus, the average calculation time for one high-fidelity operating condition is approximately 2.50 min. In contrast, after the XGBoost surrogate model is trained, the prediction time for a new operating condition is substantially reduced, allowing the model to replace a large number of repeated thermodynamic iteration calculations.

The coefficient of determination (R^2), mean absolute error (MAE), root mean square error (RMSE), and mean absolute percentage error (MAPE) are used as evaluation metrics. Among them, R^2 characterizes how well the model fits the variation trends of the reference data, with a value closer to 1 indicating better fitting performance; MAE represents the mean absolute deviation between predicted and reference values; RMSE reflects the model sensitivity to larger deviations; and MAPE describes the mean percentage error of the prediction relative to the reference value. The evaluation results are presented in Table 1.

Table 1. Validation results of the surrogate model.

Output variable	R^2	MAE	RMSE	MAPE/%
Round-trip efficiency	0.9926	0.0094	0.0145	1.210
Net electrical efficiency	0.9799	0.0024	0.0033	0.426
Net specific work	0.9857	1.5847	2.1613	0.459

5. Case Analysis and Results Discussion

5.1. Case Analysis

A typical operating case is analyzed to verify the performance advantages of the integrated system. Seawater at 10 °C is selected as the cold source, and the main initial input parameters are listed in Table 2.

Table 2. Basic parameters of case analysis.

Parameter	Value	Parameter	Value
Low-pressure tank pressure	7.4 MPa	First-stage compressor inlet temperature	40 °C
High-pressure tank pressure	30.3 MPa	First-stage compressor outlet pressure	7.4 MPa
Storage temperature	20 °C	Minimum heat-transfer temperature difference	5 °C
Low-pressure tank mass flow rate	500 kg/s	Turbine inlet pressure	30 MPa
Fuel mass flow rate	16.5 kg/s	Turbine outlet pressure	3.4 MPa
Combustor outlet temperature	1150 °C	Compressor isentropic efficiency	0.9
Total CO_2 circulating flow rate	1292.4 kg/s	Pump isentropic efficiency	0.85
Turbine inlet mass flow rate	1271.6 kg/s	Turbine isentropic efficiency	0.89
Generator efficiency	0.995	Lower heating value (LHV)	46.502 $MJ·kg^{-1}$

Based on the parameters listed in Table 2, the system performance under the three operating modes is calculated, and the results are shown in Table 3. The round-trip efficiency of the integrated system is 85.74%, indicating that the energy loss during the charging-discharging process is relatively small and that the energy input during charging can be effectively recovered and utilized.

Table 3. Calculation results of case analysis.

Parameter	Unit	Normal mode	Charging mode	Discharging mode
Turbine output power	MW	620.44	620.44	860.42
Total compression power consumption	MW	100.12	138.86	3.78
Fuel thermal input	MW	768.31	768.31	1073.58
System net electric power	MW	423.15	384.62	624.33
Net electrical efficiency	%	55.08	50.06	58.15
Net specific work	$kJ·kg^{-1}$	332.78	302.48	353.67

Table 3. (continued)

Parameter	Unit	Normal mode	Charging mode	Discharging mode
RTE	%	–	–	85.74
System net shaft power	MW	425.28	386.55	627.47

To further demonstrate the performance advantages of coupling the Allam cycle with the CO_2 energy storage system, the integrated system is compared with a conventional Allam cycle and an independent CO_2 energy storage system, as shown in Table 4. The conventional Allam cycle has a net electrical efficiency of 55.08% and a net specific work of 332.78 kJ/kg; the independent CO_2 energy storage system has a round-trip efficiency of 67.25%; and the integrated system proposed in this paper achieves a net electrical efficiency, round-trip efficiency, and net specific work of 58.15%, 85.74%, and 353.67 kJ/kg, respectively.

Table 4. Performance comparison between the integrated system and independent systems.

System type	Net electrical efficiency/%	Round-trip efficiency/%	Net specific work/kJ·kg^{-1}
Conventional Allam cycle	55.08	–	332.78
CO_2 energy storage system	–	67.25	–
Integrated system	58.15	85.74	353.67

5.2. Results Discussion

To further reveal the effects of key operating parameters on the performance of the integrated system, single-factor sensitivity analyses are carried out for the first-stage compressor outlet pressure, turbine cooling-flow temperature, and tank mass flow rate based on the trained XGBoost surrogate model. The round-trip efficiency (RTE), net electrical efficiency, and net specific work are used as performance indicators.

As shown in Figure 5, the Comp1 outlet pressure has a significant influence on system performance, and its effects on different performance indicators are opposite in direction. As the Comp1 outlet pressure increases from 7.4 MPa to 11.0 MPa, the round-trip efficiency rises from 86.26% to 89.22%, corresponding to an overall increase of approximately 3.4%. The net electrical efficiency decreases from 57.91% to 56.00%, with a decrease of approximately 3.3%, while the net specific work decreases from 352.76 kJ/kg to 340.68 kJ/kg, with a decrease of approximately 3.4%. This indicates that increasing the Comp1 outlet pressure is beneficial for enhancing the overall energy recovery capability of the system, but it weakens the power-generation performance during discharging.

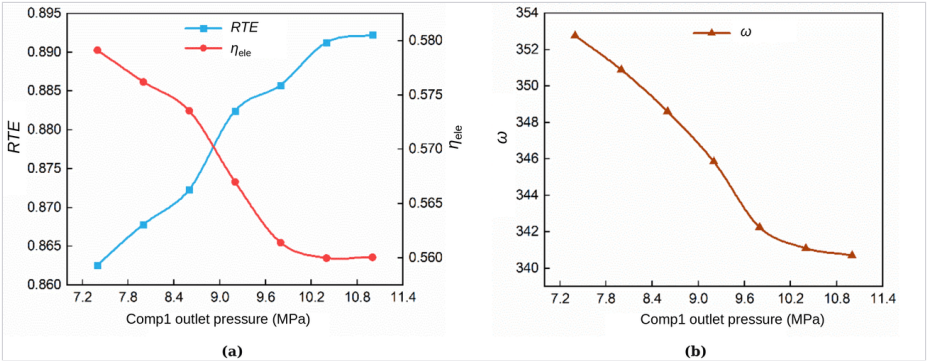

Figure 5. Effects of Comp1 outlet pressure on the integrated system: (a) round-trip efficiency and net electrical efficiency; (b) net specific work.

As shown in Figure 6, the turbine cooling-flow temperature also has a significant influence on system performance, with opposite effects on round-trip efficiency and power-generation performance. As the cooling-flow temperature increases from 200 °C to 500 °C, the round-trip efficiency decreases from 86.22% to 79.93%, corresponding to an overall decrease of approximately 7.3%. In contrast, the net electrical efficiency increases from 57.99% to 58.91%, with an increase of approximately 1.6%, and the net specific work increases from 352.79 kJ/kg to 360.19 kJ/kg, with an increase of approximately 2.1%. This indicates that increasing the cooling-flow temperature improves the power-generation performance during discharging but reduces the overall energy recovery capability of the system.

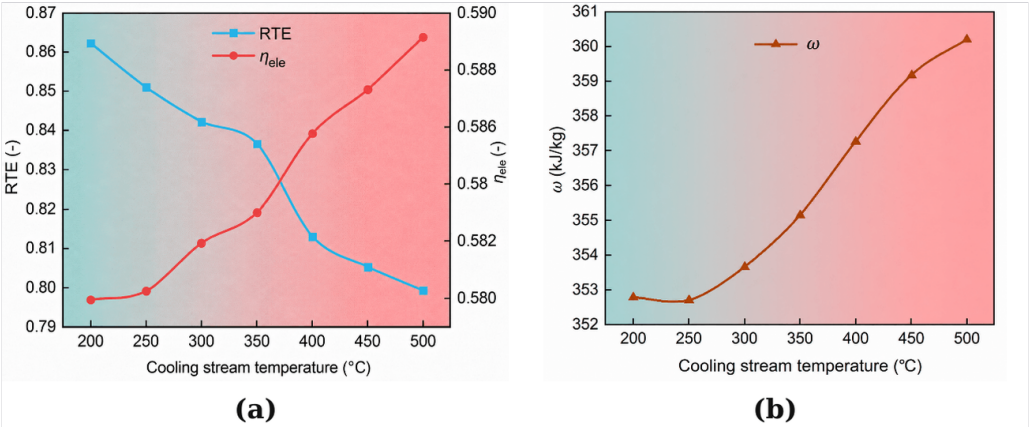

Figure 6. Effect of turbine cooling-flow temperature on the integrated system: (a) round-trip efficiency and net electrical efficiency; (b) net specific work.

As shown in Figure 7, the tank mass flow rate has a nonlinear effect on system performance. As the tank mass flow rate increases from 400 kg/s to 600 kg/s, the round-trip efficiency changes only slightly overall and exhibits an initial increase followed by a decrease, reaching a relatively high level near 440-480 kg/s, with a maximum of approximately 86.32%. The net electrical efficiency increases from 57.67% to 58.49%, with an increase of approximately 1.4%, while the net specific work increases from 350.85 kJ/kg to 356.64 kJ/kg, with an increase of approximately 1.6%. This indicates that moderately increasing the tank mass flow rate is conducive to improving the net electrical efficiency and net specific work, but its improvement in the overall energy recovery capability is limited. When the flow rate is too high, the round-trip efficiency slightly decreases instead.

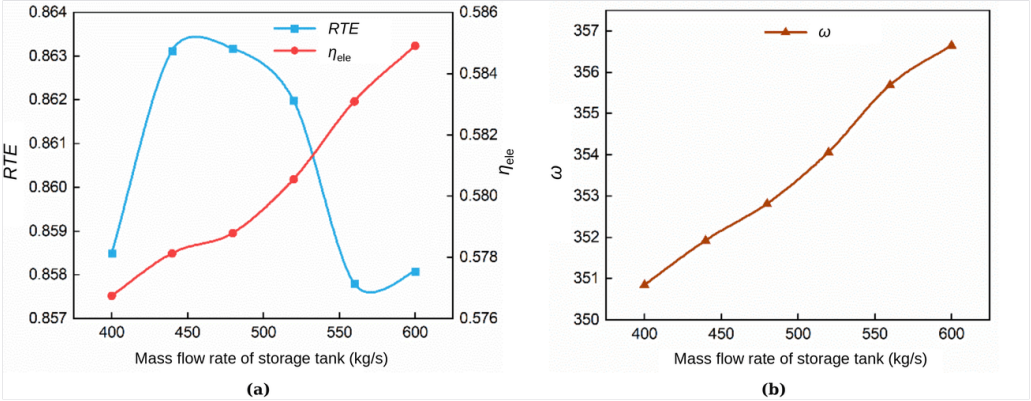

Figure 7. Effect of tank mass flow rate on the integrated system: (a) round-trip efficiency and net electrical efficiency; (b) net specific work.

6. Conclusion

This paper proposes a novel integrated system coupling an Allam cycle with CO_2 energy storage, in which the stored CO_2 participates in the pressurization, recuperation, and discharging processes within the Allam cycle. A CO_2 stream routing control mechanism is established for the normal, charging, and discharging modes, enabling flexible switching among power generation, energy storage, and peak-shaving conditions. An XGBoost-based machine-learning surrogate model is developed to rapidly predict the round-trip efficiency, net electrical efficiency, and net specific work under multi-parameter variations, thereby improving the efficiency of multi-condition performance evaluation. The case analysis shows that, compared with the conventional Allam cycle, the integrated system increases the net electrical efficiency by 3.57 percentage points, achieves an energy storage round-trip efficiency of 85.74%, and increases the net specific work by 6.28%. Based on this, the effects of different operating parameters on system performance are further analyzed. The main conclusions are as follows:

- The XGBoost surrogate model predicts the round-trip efficiency, net electrical efficiency, and net specific work with high accuracy. The R^2 values on the validation set reach 0.9926, 0.9799, and 0.9857, respectively, indicating that the surrogate model can accurately characterize the nonlinear relationship between input parameters and system performance.
- As the Comp1 outlet pressure increases, the system round-trip efficiency rises to 89.22%, with an increase of approximately 3.4%. However, both the net electrical efficiency and the net specific work decrease, with reductions of approximately 3.3% and 3.4%, respectively. This indicates that increasing this pressure helps enhance system energy recovery capability, but it weakens system output performance to some extent, and the magnitude of its positive effect on round-trip efficiency is generally comparable to its negative effect on net electrical efficiency.
- The turbine cooling-flow temperature has a significant effect on system performance. As the cooling-flow temperature increases, the round-trip efficiency decreases by approximately 7.3%, while the net electrical efficiency and net specific work increase by approximately 1.6% and 2.1%, respectively. This indicates that this parameter has a stronger influence on the system round-trip efficiency than on the net electrical efficiency and net specific work.
- The tank mass flow rate has a relatively weak influence on system performance. Increasing the tank mass flow rate can improve the net electrical efficiency and net specific work to a certain extent, but its improvement in round-trip efficiency is limited, and the overall response exhibits weak nonlinearity.

Declarations

Author contributions. Yingzong Liang: Writing (original draft), Data curation, Formal analysis, Investigation, Methodology, Conceptualization. Jialuan Zhang: Writing (review and editing). Xianglong Luo: Writing (review and editing).

Funding. This research received no specific funding.

Conflicts of interest. The authors declare no competing interests.

Data availability. The data that support the findings of this study are available from the corresponding author upon reasonable request.

References

Allam, R.J.; Palmer, M.; Brown, G.W. (2013) *System and method for high efficiency power generation using a carbon dioxide circulating working fluid*. Patent. Google Patents.

Crippa, M.; Guizzardi, D.; Banja, M.; Solazzo, E.; Muntean, M.; Schaaf, E.; Pagani, F.; Monforti-Ferrario, F.; Olivier, J.G.J.; Quadrelli, R.; Risquez Martin, A.; Taghavi-Moharamli, P.; Grassi, G.; Rossi, S.; Oom, D.; Branco, A.; San-Miguel, J.; Vignati, E. (2022) *CO_2 emissions of all world countries: JRC/IEA/PBL 2022 report*. EUR 31182 EN. Luxembourg: Publications Office of the European Union. Available at: https://doi.org/10.2760/07904

Li, Bo; Xu, Hongpeng; Jiang, Yuemao; Wu, Chuang; Wang, Shun-sen (2025) 'Energy, exergy, economic and exergoeconomic (4E) analysis of a high-temperature liquid CO_2 energy storage system: Dual-stage thermal energy storage for performance enhancement', *Renewable Energy*, 239, pp. 122069. Available at: https://doi.org/10.1016/j.renene.2024.122069

Scaccabarozzi, Roberto; Gatti, Manuele; Martelli, Emanuele (2016) 'Thermodynamic analysis and numerical optimization of the NET Power oxy-combustion cycle', *Applied Energy*, 178, pp. 505-526. Available at: https://doi.org/10.1016/j.apenergy.2016.06.060

Sun, Wenxu; Liu, Xu; Yang, Xuqing; Yang, Xiaohu; Liu, Zhan (2021) 'Design and thermodynamic performance analysis of a new liquid carbon dioxide energy storage system with low pressure stores', *Energy Conversion and Management*, 239, pp. 114227. Available at: https://doi.org/10.1016/j.enconman.2021.114227

HOW TO CITE THIS PAPER

Liang, Y., Zhang, J. and Luo, X. (2026). Machine-Learning-Assisted Design and Analysis of an Integrated Allam Cycle-CO_2 Energy Storage System. In: *Proceedings of the 22nd International Conference on Sustainable Energy Technologies (SET2026)*, Kuala Lumpur, Malaysia, 13 to 15 August 2026. Caravel Press, pp. 379–390. ISBN 978-1-995850-00-9. ISSN 2978-4387. https://doi.org/10.65582/set.2026.032

COPYRIGHT AND LICENCE

© 2026 The Author(s). This is an open access paper distributed under the terms of the Creative Commons Attribution (CC BY 4.0) licence, which permits unrestricted use, distribution and reproduction in any medium, provided the original work is properly cited.

WSSET World Society of Sustainable Energy Technologies Organised by the World Society of Sustainable Energy Technologies. Published by Caravel Press.